Signal-Selective Time-Difference-of-Arrival Estimation for Passive Location of Man-Made Signal Sources in Highly Corruptive Environments, Part II: Algorithms and Performance

Chih-Kang Chen, *Member, IEEE,* and William A. Gardner, *Fellow, IEEE*

Abstract—**For the problem of estimating time difference of arrival (TDOA) of radio waves impinging on a pair of antennas for the purpose of passively locating the source of a communications or telemetry signal in the presence of interfering signals and noise, a new class of signal-selective algorithms that are highly tolerant to interference and noise is introduced. In part I of this two-part paper, the background theory of cyclostationary signals is presented and applied to the design of various new TDOA methods. In this part II, algorithmic implementations are described and their performance capabilities are assessed by analysis and simulation. By virtue of the fact that the multiple-signal resolution problem is essentially eliminated by the signal selectivity of the algorithms, two performance advantages are gained: 1) the practicality of source location with relatively closely spaced antennas is substantially enhanced, and 2) the problem of sorting through multiple TDOA estimates, resulting from multiple interferers, for the estimate corresponding to a particular signal of interest is eliminated. These new algorithms exhibit their signal selectivity regardless of the extent of temporal, spectral, or spatial overlap among received signals. It is only required that the signal of interest have a known (or measurable) analog carrier frequency or digital keying rate that is distinct from those of all interfering signals. Yet the computational complexity of these algorithms is no more than that of conventional generalized cross-correlation algorithms.**

I. Introduction

In part I of this paper [1], a new class of signal-selective methods for time-difference-of-arrival (TDOA) estimation is introduced. The signal selectivity gained by exploitation of the cyclostationary property of the signals of interest, as reflected in the spectral correlation functions for the received data, promises substantial tolerance to additive noise and interfering signals regardless of temporal, spectral, and spatial overlap. The purpose of this paper, part II, is to introduce algorithmic implementations of some of the new methods and to corroborate the theoretical arguments given in part I by quantitative evaluation of their performance.

In Section II, specific algorithms for digital implementation of the various methods are described, and practical considerations for implementation are discussed. This includes the issues involved in choosing spectral-smoothing-window widths and temporal-integration intervals for estimating the spectral correlation functions. In Section III, four distinct noise and interference environments are defined and a qualitative discussion of the performance of the various algorithms in these environments is given and illustrated with graphical descriptions of the TDOA estimation functions produced by the algorithms. In Section IV, the performance of the algorithms in the various environments is quantitatively measured in terms of mean-squared error obtained from Monte Carlo simulations. Finally, in Section V, conclusions are drawn.

For easy reference, this introduction is concluded with formulas specifying the TDOA estimate $\hat{D}$ obtained from each of the methods to be evaluated.[1]

Conventional Generalized Cross-Correlation Method (GCC):

$$\hat{D} = \arg\max_{\tau} \{\hat{b}_0(\tau)\} \tag{1}$$

where $\hat{b}_0(\tau)$ is an estimate of

$$b_0(\tau) \triangleq \int_{||f|-f_0|<B_0/2} \frac{S_{yx}^0(f)}{S_x^0(f)} e^{i2\pi f\tau}\, df \tag{2}$$

and f_0 and B_0 are the center frequency and bandwidth of the power spectral density $S_s^0(f)$ of the signal of interest.

Spectral Correlation Ratio Method (SPECCORR):

$$\hat{D} = \arg\max_{\tau} \{\hat{b}_\alpha(\tau)\} \tag{3}$$

Manuscript received May 6, 1991; revised April 5, 1991. This work was supported jointly by ESL, Inc., with partial matching support from the California State MICRO Program, and the Army Research Office sponsored by the United States Army Communications Electronics Command Center for Signals Warfare under Contract DAAL03-89-C-0035.

C.-K. Chen is with Silicon Engines, Palo Alto, CA 94303.

W. A. Gardner is with the Department of Electrical Engineering and Computer Science, University of California, Davis, CA 95616.

IEEE Log Number 9106571.

[1]The primes used on the symbols in (5)–(10) originated in [1] and are retained here for consistency.

where $\hat{b}_\alpha(\tau)$ is an estimate of

$$b_\alpha(\tau) \triangleq \left| \int_{||f|-f_\alpha|<B_\alpha/2} \frac{S_{yx}^\alpha(f)}{S_x^\alpha(f)} e^{i2\pi f\tau}\, df \right| \tag{4}$$

and f_α and B_α are the center and width of the spectral correlation function $S_s^\alpha(f)$ if known, in which case the prefix BL (for band limited) is used with acronym the SPECCORR; otherwise, f_α and B_α must be chosen to cover the entire band where $S_s^\alpha(f)$ might reside.

Spectral Coherence Alignment Method (SPECCOA)—Also the Spectral Correlation Product Method (SPECCORP):

$$\hat{D} = \arg\max_\tau \{\hat{c}'_\alpha(\tau)\} \tag{5}$$

where $\hat{c}'_\alpha(\tau)$ is an estimate of

$$c'_\alpha(\tau) = \mathrm{Re}\left\{ \int_{|f|<B} S_{yx}^\alpha(f) S_x^\alpha(f)^* e^{i2\pi(f+\alpha/2)\tau}\, df \right\} \tag{6}$$

and B is the entire analysis band of the receiver.[2]

Spectral Coherence Nulling Method (SPECCON):

$$\hat{D} = \arg\min_\tau \{\hat{d}'_\alpha(\tau)\} \tag{7}$$

where $\hat{d}'_\alpha(\tau)$ is an estimate of

$$\begin{aligned} d'_\alpha(\tau) \triangleq \mathrm{Re}\Bigg\{ \int_{|f|<B} \Big[& S_x^\alpha(f) S_y^\alpha(f)^* e^{-i2\pi\alpha\tau} \\ & + S_{yx}^\alpha(f)^* S_{xy}^\alpha(f) e^{-i4\pi f\tau} \\ & - [S_x^\alpha(f)^* S_{xy}^\alpha(f) + S_y^\alpha(f) S_{yx}^\alpha(f)^*] \\ & \cdot e^{-i2\pi(f-\alpha/2)\tau} - [S_x^\alpha(f) S_{yx}^\alpha(f)^* \\ & + S_y^\alpha(f)^* S_{xy}^\alpha(f)]\, e^{-i2\pi(f+\alpha/2)\tau} \Big]\, df \Bigg\}. \end{aligned} \tag{8}$$

Postprocessed SPECCON Method (PP-SPECCON):

$$\hat{D} = \arg\max_\tau \{\hat{d}''_\alpha(\tau)\} \tag{9}$$

where $\hat{d}''_\alpha(\tau)$ is the estimate

$$\hat{d}''_\alpha(\tau) \triangleq \hat{d}'_\alpha(\tau) \circledast \overline{d'_\alpha(\tau)} \tag{10a}$$

in which $\circledast$ denotes correlation and

$$\overline{d'_\alpha(\tau)} = \begin{cases} \mathrm{Re}\left\{ \int |S_s^\alpha(f)|^2 [e^{-i2\pi\alpha\tau} + e^{-i4\pi f\tau} \right. \\ \qquad \left. - 2e^{-i2\pi(f-\alpha/2)\tau} - 2e^{-i2\pi(f+\alpha/2)\tau}]\, df \right\}, \\ \qquad |\tau| \le 1/2\alpha \\ 0, \qquad |\tau| > 1/2\alpha. \end{cases} \tag{10b}$$

[2]The version (6) of SPECCOA is optimum for real data, whereas the version (4) of SPECCORR is optimum for complex data (cf. [1]). Nevertheless, (4) is useful for real data and was used in the simulations reported in this paper, which were performed before this distinction was recognized.

In these formulas, $S_x^\alpha(f)$, $S_y^\alpha(f)$, and $S_{xy}^\alpha(f)$ are the ideal autospectral and cross-spectral correlation functions for the data $x(t)$ and $y(t)$ received at the two antennas (cf. [1, sec. II, III]). As explained in the next section, in all simulations considered, α is chosen to be the keying rate of the binary phase-shifted-keyed (BPSK) signal of interest (SOI), cf. [1, appendix] and Section III. Also, in order to separate the effects on performance of channel- and receiver-mismatch, we have simulated the more idealized model in which the two received signals have equal scale factors ($A = 1$ in [1, eq. (38)]).

II. Implementation

In practice, the ideal spectral correlation functions $S_x^\alpha(f)$, $S_y^\alpha(f)$, and $S_{xy}^\alpha(f)$ that are used by the methods summarized in Section I must be replaced by their estimates obtained from measurements. Computationally efficient estimates are obtained using the frequency smoothed cyclic periodograms [2, chs. 13, 15], [3]:

$$S_{yxT}^\alpha(f)_{\Delta f} = \frac{1}{\Delta f} \int_{f-\Delta f/2}^{f+\Delta f/2} S_{yxT}^\alpha(\nu)\, d\nu \tag{11a}$$

where

$$S_{yxT}^\alpha(f) = \frac{1}{T} Y_T(f+\alpha/2) X_T^*(f-\alpha/2) \tag{11b}$$

and

$$S_{xT}^\alpha(f)_{\Delta f} = \frac{1}{\Delta f} \int_{f-\Delta f/2}^{f+\Delta f/2} S_{xT}^\alpha(\nu)\, d\nu \tag{12a}$$

where

$$S_{xT}^\alpha(f) = \frac{1}{T} X_T(f+\alpha/2) X_T^*(f-\alpha/2) \tag{12b}$$

in which

$$X_T(f) = \int_{-T/2}^{T/2} x(t) e^{-i2\pi ft}\, dt. \tag{12c}$$

In (11) and (12), T is the integration, or collection, time and Δf is the width of the frequency smoothing window. The FFT algorithm is used to obtain discrete-time/discrete-frequency transforms corresponding to the transforms $X_T(f)$ and $Y_T(f)$. Of course, complete immunity to noise and interference can only be obtained in the limit as the integration time T approaches infinity. However, for finite but sufficiently large T, substantial tolerance to such corruption can be obtained because the inequalities

$$\begin{aligned} |S_{nT}^\alpha(f)_{\Delta f}| &\ll |S_{sT}^\alpha(f)_{\Delta f}| \quad \text{and} \\ |S_{mT}^\alpha(f)_{\Delta f}| &\ll |S_{sT}^\alpha(f)_{\Delta f}| \end{aligned} \tag{13}$$

can then be satisfied, assuming that the smoothing product is sufficiently large, i.e., at least $T\Delta f \gg 1$ [2, Ch. 15].

In (13), $n(t)$ and $m(t)$ represent all additive corruption (noise and interfering signals) to the signals of interest $s(t)$ and $s(t - D)$ contained in the data $x(t)$ and $y(t)$ received by the two antennas.

The integration time T is constrained by the coherence time of cyclostationarity (e.g., the coherence time, or reciprocal of the bandwidth, of a sine-wave carrier or of the fundamental frequency of a keying-clock signal), the reciprocal of the cycle frequency spreading width due to any time-varying Doppler shift that might occur, and the reciprocal of the error in knowledge of the cycle frequency α, but it can often be made large enough to accommodate quite low signal-to-interference-and-noise ratios (SINR's). The choice of the frequency smoothing window-width Δf must satisfy two opposing conditions. It must be large enough to render sufficient reliability of the spectral correlation function estimates, e.g., $\Delta f >> 1/T$ (not to exceed the bandwidth of the spectral correlation function of the signal, of course), and yet it must be small enough to resolve the oscillation in the cross spectral correlation function due to the TDOA. Specifically, it can be shown [2, Ch. 15] that the temporal mean of the estimate (11a) of the cross spectral correlation function is given by

$$\text{mean}\,\{S^{\alpha}_{yxT}(f)_{\Delta f}\} = S^{\alpha}_{yx}(f) \otimes E(f) = [S^{\alpha}_{s}(f)e^{-i2\pi(f+\alpha/2)D}] \otimes E(f) \quad (14)$$

where $\otimes$ denotes convolution and $E(f)$ is the effective frequency smoothing window

$$E(f) = \frac{1}{T}|W_{1/T}(f)|^2 \otimes V_{\Delta f}(f) \quad (15)$$

in which $W_{1/T}(f)$ is the Fourier transform of the data tapering window used in computing the Fourier transforms $X_T(f)$ and $Y_T(f)$, and $V_{\Delta f}(f)$ is the spectral smoothing window used (e.g., the rectangle in (11a) and (12a)). The width of $E(f)$ is approximately Δf. It follows from (14) that the frequency smoothing window width Δf should not greatly exceed $1/2D$ in order to avoid destructive leakage effects due to the oscillatory factor resulting from time misalignment, $D \neq 0$. If the TDOA D is too large and the two conditions $\Delta f >> 1/T$ and $\Delta f < 1/2D$ cannot be satisfied simultaneously, a two-stage TDOA estimation procedure can be employed. In the first stage, we choose $\Delta f < 1/2D$ (using an upper bound on the unknown D) and use the relatively low-reliability spectral correlation function estimates (resulting from $T >> 1/\Delta f$) to obtain a coarse TDOA estimate $\hat{D}_1$. Then, in the second stage, this $\hat{D}_1$ is subtracted from the true TDOA D (i.e., by delaying $x(t)$ in time by the amount $\hat{D}_1$) and a larger smoothing window width, $\Delta f < 1/(2|D - \hat{D}_1|)$, is used to obtain more reliable spectral correlation function estimates to get a second and finer TDOA estimate $\hat{D}_2$. Thus, the final TDOA estimate is $\hat{D} = \hat{D}_1 + \hat{D}_2$.

The condition $T\,\Delta f >> 1$ is only adequate when the SINR is not too low. That is, it can be shown [2, Ch. 15] that the temporal mean of $S^{\alpha}_{nT}(f)_{\Delta f}$ is zero and its temporal variance has the approximate proportionality[3]

$$\text{var}\,\{S^{\alpha}_{nT}(f)_{\Delta f}\} \propto \frac{1}{T\Delta f} S_n(f + \alpha/2)\, S_n(f - \alpha/2), \quad T\,\Delta f >> 1 \quad (16)$$

and the temporal mean of $S^{\alpha}_{sT}(f)_{\Delta f}$ is proportional to the product of power spectral densities (PSD's) of the signal,

$$\text{mean}\,\{S^{\alpha}_{sT}(f)_{\Delta f}\} \propto [S_s(f + \alpha/2)S_s(f - \alpha/2)]^{1/2} \quad (17)$$

(with the proportionality factor equal to the spectral self-coherence $C^{\alpha}_{s}(f)$ of the signal, cf. [1, eq. (27)]). Thus, the integration time T required to satisfy (13) at each frequency f is approximately inversely proportional to the product of PSD-SINR's:

$$T \propto |C^{\alpha}_{s}(f)|^{-1}\left[\frac{S_s(f + \alpha/2)S_s(f - \alpha/2)}{S_n(f + \alpha/2)S_n(f - \alpha/2)}\right]^{-1}. \quad (18)$$

It follows that T must increase twice as fast as the SINR decreases (e.g., T must be quadrupled for every reduction by one half of SINR).

Let us now return to the issue of the effect of error in the cycle frequency α on the choice of integration time T. If the cycle frequency is unknown or not precisely known, for example, due to Doppler shifts, then an estimate must be used. Since the cycle resolution of the spectral correlation function estimate (11) is $\Delta\alpha = 1/T$ (cf. [2, ch. 13]), then the required accuracy of the estimate of α increases as the averaging time T increases so that the estimated α lies within $\pm\Delta\alpha/2 = \pm 1/2T$ of the cycle frequency of the SOI. One way to estimate the cycle frequency of interest is to compute the cyclic autocorrelation function, as a function of α, with a finite averaging time T_* for one or several fixed lag values τ. This can be easily accomplished by use of a DFT (or FFT) operating on the lag product $x(t - \tau)x(t)^*$. The accuracy of the estimate obtained using this method is, obviously, limited to $\Delta\alpha = 1/T_*$.

It is also of importance in selecting an averaging time T to consider the possibility of a cycle frequency of an interferer α_i that lies close to the cycle frequency of the signal of interest α, which is used by the cyclostationarity-exploiting method. In this situation, we require that $1/T = \Delta\alpha < |\alpha_s - \alpha_i|$ in order to resolve the two cycle frequencies and reduce the contribution from the spectral correlation of the interference which can degrade the spectral correlation function estimate and consequently the TDOA estimate (cf. [2]). However, even when the preceding resolution inequality is satisfied, cycle leakage can still degrade performance. For a given integration time T, the degree of cycle leakage can be controlled to some ex-

[3]This is an accurate approximation for stationary Gaussian noise, but requires minor modification (e.g., by a factor of 2) for non-Gaussian and/or cyclostationary interferers.

tent through the use of a windowing technique. The cyclic autocorrelation

$$R_x^\alpha(\tau) \triangleq \lim_{T\to\infty} \frac{1}{T} \int_{-T/2}^{T/2} x(t + \tau/2)x^*(t - \tau/2)e^{-i2\pi\alpha t}\, dt \tag{19}$$

which is the inverse Fourier transform of the spectral correlation function $S_x^\alpha(f)$, is a Fourier coefficient of the periodic autocorrelation

$$R_x(t, \tau) = \sum_\alpha R_x^\alpha(\tau)e^{i2\pi\alpha t} \tag{20}$$

(see [1, sec. II]), and is nonzero at α equal to the cycle frequencies of the signal, e.g., $\alpha = \alpha_s$, and cycle frequencies of the interfering signals, e.g., $\alpha = \alpha_i$. In other words, $|R_x^\alpha(\tau)|^2$ is the power in the spectral line at frequency α in the power spectrum of the lag-product waveform $z_\tau(t) \triangleq x(t + \tau/2)x^*(t - \tau/2)$ for fixed τ. Even though the cycle resolution might be smaller than the separation between the cycle frequencies of the signal and interference, $\Delta\alpha = 1/T < |\alpha_s - \alpha_i|$, strong spectral correlation of the interference at $\alpha = \alpha_i$ can still leak into the spectral correlation measurements for the signal at $\alpha = \alpha_s$ [2]. Thus, if a proper tapering window for the lag product waveform $z_\tau(t)$ is used in (19) when integration time is finite, the cycle leakage can be reduced to some extent. It can be shown [2, ch. 13, sec. A] that using a tapering window directly on the data $x(t)$ (and $y(t)$) in (12c) is also helpful.

Another possible source of performance degradation is channel mismatch, e.g., due to multipath propagation. If the channel from the source to (and including) the sensor producing the data $x(t)$ has transfer function $A(f)$ and that from the source to the sensor producing $y(t)$ has transfer function $B(f)$, then the model [1, eq. (38)] must be generalized to

$$x(t) = a(t) \otimes s(t) + n(t) \tag{21a}$$

$$y(t) = b(t) \otimes s(t) + m(t). \tag{21b}$$

Consequently, the autospectral and cross-spectral correlation functions [1, eq. (40)] are generalized to

$$S_x^\alpha(f) = A(f + \alpha/2)A^*(f - \alpha/2)S_s^\alpha(f) + S_n^\alpha(f) \tag{22}$$

$$S_{yx}^\alpha(f) = B(f + \alpha/2)A^*(f - \alpha/2)S_s^\alpha(f) \cdot e^{-i2\pi(f+\alpha/2)D} + S_{mn}^\alpha(f). \tag{23}$$

Under the condition [1, eq. (42)] that α is a cycle frequency in $s(t)$ but not in $n(t)$ and $m(t)$, this generalization results in the SPECCORR formula

$$\frac{S_{yx}^\alpha(f)}{S_x^\alpha(f)} = \frac{B(f + \alpha/2)}{A(f + \alpha/2)} e^{-i2\pi(f+\alpha/2)D} \tag{24}$$

and the SPECCOA formula

$$S_{yx}^\alpha(f)S_x^\alpha(f)^* = |A(f - \alpha/2)|^2|S_s^\alpha(f)|^2B(f + \alpha/2) \cdot A^*(f + \alpha/2)\, e^{-i2\pi(f+\alpha/2)D}. \tag{25}$$

In both cases (24) and (25), the phase function $\Phi(f)$ becomes

$$\Phi(f) = -2\pi(f + \alpha/2)D + \arg\{B(f + \alpha/2)\} - \arg\{A(f + \alpha/2)\}. \tag{26}$$

Thus, any mismatch in the phase versus frequency characteristics of the two channels will modify the linear phase characteristic and thereby degrade the TDOA estimate. Since the amount of degradation depends critically on the particular type of channel mismatch and since such mismatch can be compensated for when $A(f)$ and $B(f)$ are independent of f as explained in [1], this effect is not considered in the simulation study presented in the following sections.

Another possible source of performance degradation is differential Doppler effect between the two reception platforms, relative to the emitter location. When the Doppler effect can be approximated as a uniform frequency shift, the TDOA algorithms in Section I can be easily compensated to accommodate differential Doppler.

For the BPSK signal of interest considered in the following sections, any one of several values for α could be used, namely, $\alpha = \alpha_k$, the keying rate, $\alpha = 2f_c$, the doubled carrier frequency, or $\alpha = 2f_c \pm \alpha_k$. Since $\alpha = 2f_c$ yields the strongest cyclic feature as shown in [1, appendix], it would result in the best performance. However, since carrier frequencies used in the transmitter are easily changed, they can be difficult for an unintended receiver to know. Consequently, $\alpha = \alpha_k$ is used in all the simulations reported in the following sections.

III. Qualitative Performance Assessment

To demonstrate the tolerance to noise and interference exhibited by the SPECCORR, SPECCOA, and SPECCON methods, we consider a real simulated BPSK signal of interest (cf. [1, appendix]) corrupted by interference for four different environments ranging from broad band to narrow band and including multiple and single interfering signals. In all cases, uncorrelated broad-band white Gaussian noises (WGN's) are also added to the two received signals. The discrete-time sampling increment is T_s. The BPSK signal has carrier frequency of $f_c = 0.25/T_s$ and keying rate of $\alpha_k = 0.0625/T_s$. It has full-duty-cycle half-cosine envelope, which results in a null-to-null bandwidth of $B = 0.1875/T_s$. The TDOA for the BPSK signal is $D = 48T_s$. For an AOA of 60° from the baseline, this value of D corresponds to a distance between receivers of $L = cD/\sin 60° = 96T_sc = 24c/f_c = 24$ wavelengths of the carrier. Any closer spacing would begin to require phase versus AOA calibration, in which case a high-resolution array might be preferable (although this would require that sensors be within half a wavelength of each other to avoid ambiguity).

For comparison with simulation results, the ideal ($T \to \infty$ and $\Delta f \to 0$ in (11)–(12)) SPECCOA function [1, eq. (68a)], SPECCON function [1, eq. (75)], and PP-SPECCON function [1, eq. (76)] with $\alpha = \alpha_k$ for this

BPSK signal are shown in [1, figs. 3 and 4]. The BL-SPECCORR function [1, = eq. (56c)] is the well-known sinc envelope on a sinusoidal oscillation, and is shown in [1, fig. 2].

A. Environment 1: Multiple Interference

In this environment, the interference consists of five AM signals with carrier frequencies of $f_1 = 0.156/T_s$, $f_2 = 0.203/T_s$, $f_3 = 0.266/T_s$, $f_4 = 0.313/T_s$, $f_5 = 0.375/T_s$, bandwidths of $B_1 = 0.04/T_s$, $B_2 = 0.05/T_s$, $B_3 = 0.045/T_s$, $B_4 = 0.04/T_s$, $B_5 = 0.08/T_s$, and corresponding TDOA's of $\tau_1 = 28T_s$, $\tau_2 = 68T_s$, $\tau_3 = 78T_s$, $\tau_4 = 38T_s$, $\tau_5 = 58T_s$. The signal-to-interference ratio (SIR) of each AM signal is 0 dB and the signal-to-noise ratio (SNR) is 0 dB, which yields a total SINR of -8 dB. The magnitude of the measured spectral correlation function $|S_x^\alpha(f)|$ for this highly corrupted BPSK signal is shown in Fig. 1(a) as the height of a surface above the plane with coordinates f and α, and that for the uncorrupted BPSK is shown in Fig. 1(b). These measurements were obtained using the discrete-time and discrete-frequency counterpart of the frequency-smoothed cyclic periodogram (12), with $T = NT_s$, $N = 32\ 768$, and smoothing product $T\,\Delta f = 1024$.

The surface along $\alpha = 0$ in Fig. 1(a) is the power spectral density function, from which it is easily seen (by comparing to Fig. 1(b)) that the signal of interest is completely masked. However, for $\alpha = \pm\,\alpha_k$, $\alpha = \pm 2f_c$, and $\alpha = \pm 2f_c \pm \alpha_k$, the spectral correlation features of the signal of interest are clearly visible. Thus, the phase information associated with any of these cycle frequencies is easily extracted for TDOA estimation.

The SPECCORR function $\hat{b}_\alpha(\tau)$, specified by (4) and (11)–(12) with $T = 32\ 768T_s$ and $\Delta f = 200/T \simeq 1/164T_s < 1/2D = 1/96T_s$, was computed and graphed for $\alpha = \alpha_k$ (using a threshold for the denominator that was exceeded 95% of the time). The result is shown in Fig. 2(b). It is clear that the dominant peak occurs at the correct TDOA value, $\tau = D = 48T_s$. But a smaller spurious peak occurs at $\tau \simeq 35T_s$. To eliminate the ambiguity caused by the presence of spurious peaks, the averaging time T could be increased. Also, it can be helpful to band limit the integrand, $S_{yxT}^{\alpha 0}(f)_{\Delta f}/S_{yT}^{\alpha 0}(f)_{\Delta f}$, as in (4), to reduce measurement noise outside the band of the signal of interest (when the location of this band is known) before inverse Fourier transforming. Fig. 2(c) shows $\hat{b}_\alpha(\tau)$ when the integrand is weighted by a raised-cosine window centered at f_c with width of $3\alpha_k$, and indeed only one peak (at the correct value of TDOA) exists in this band-limited (BL) SPECCORR function, although it occurs within an oscillatory burst. In contrast to this, we see from the graph of $\hat{b}_0(\tau)$ in Fig. 2(a) for $\alpha = 0$, which corresponds to the conventional GCC method based on (2), that the peak of interest is only one of many peaks, any one of which might be taken as the TDOA estimate. Although the conventional GCC method is somewhat immune to narrow-band interference (see environment 4), we see that it fails in this case where multiple moderate-bandwidth interferences are present.

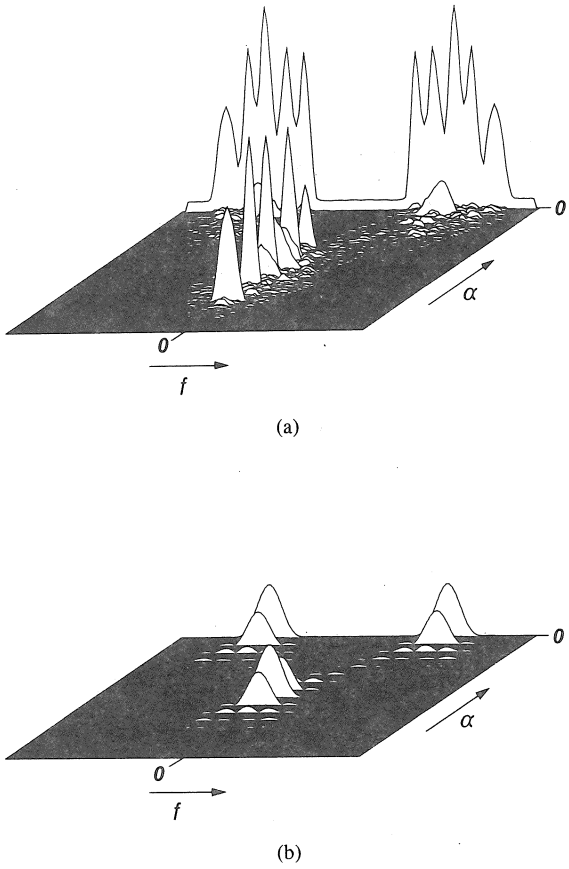

Fig. 1. (a) Magnitude of the measured spectral correlation function (on the half-plane) for received data for environment 1 (consisting of five AM SNOI, the BPSK SOI, and WGN). (Measurement parameters: $T = 32\ 768T_s$ and $T\,\Delta f = 1024$.) (b) Magnitude of the measured spectral correlation function for the BPSK SOI only. (Measurement parameters: $T = 32\ 768T_s$ and $T\,\Delta f = 1024$.)

For the SPECCOA function $\hat{c}'_\alpha(\tau)$, specified by (6), the averaging time T is reduced by a factor of 8 from $32\ 768T_s$ to $4096T_s$, and the smoothing product $T\,\Delta f$ is thereby reduced from 200 to 25 (to render the same Δf used earlier). The resultant SPECCOA function for $\alpha = \alpha_k$ is shown in Fig. 2(d). Although the measured spectral correlation function is noisier for this averaging time than for the longer one, the SPECCOA pattern shown in [1, fig. 3(b)] is clearly visible and the highest peak is at the correct value of TDOA.

The averaging time and smoothing product used for the SPECCON function $\hat{d}'_\alpha(\tau)$, specified by (8), and the PP-SPECCON function $\hat{d}''_\alpha(\tau)$, specified by (8) and (10), is the same as that for the SPECCOA method. The resultant SPECCON function for $\alpha = \alpha_k$ is shown in Fig. 2(e). Though the SPECCON pattern shown in [1, fig. 4(a)] is visible, it is not surprising, as discussed in [1], that the lowest null occurs at $\tau = 50T_s$, which is not the correct value of TDOA. However, for the PP-SPECCON function shown in Fig. 2(f), the highest peak does indeed occur at the correct value of TDOA.

For the following environments, the values for the in-

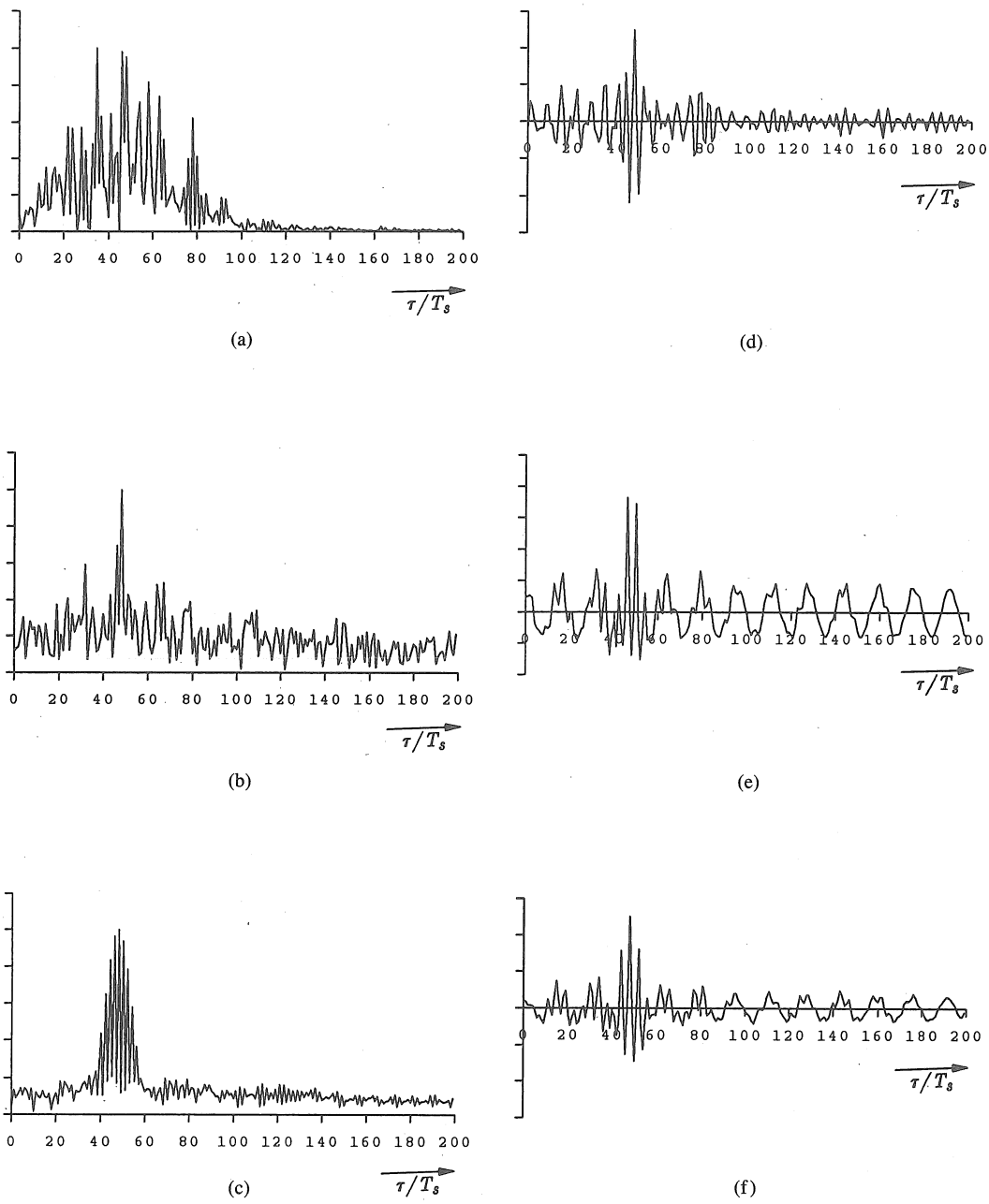

Fig. 2. (a) The GCC function $\hat{b}_0(\tau)$ (without band limiting) for environment 1. (b) The SPECCORR function $\hat{b}_\alpha(\tau)$ (without band limiting) for environment 1. The dominant peak occurs at $\tau = D = 48T_s$. (c) The BL-SPECCORR function $\hat{b}_\alpha(\tau)$ for environment 1. The highest peak occurs at $\tau = D = 48T_s$. (d) The SPECCOA function $\hat{c}'_\alpha(\tau)$ for environment 1. The highest peak occurs at $\tau = D = 48T_s$. The integration time is reduced by a factor of 8 from that used for Figs. 4(a)–(c). (e) The SPECCON function $\hat{d}'_\alpha(\tau)$ for environment 1. The lowest null occurs at $\tau = 52T_s$. The integration time is reduced by a factor of 8 from that used for Figs. 4(a)–(c). (f) The PP-SPECCON function $\hat{d}''_\alpha(\tau)$ for environment 1. The highest peak occurs at $\tau = D = 48T_s$. The integration time is reduced by a factor of 8 from that used for Figs. 4(a)–(c).

tegration, or collection, time T and the smoothing product $T\,\Delta f$ are the same as those used in environment 1.

B. Environment 2: Wide-Band Interference

The interfering signal is this environment is a BPSK signal like the signal of interest but with carrier frequency of $f_1 = 0.21875T_s$, keying rate of $\alpha_1 = 0.10/T_s$, and TDOA of $\tau_1 = 58/T_s$. It also has full-duty-cycle half-cosine envelope which yields a bandwidth of $B_1 = 0.3/T_s$. Note that even though the interference is the same type of signal as the signal of interest, it does not exhibit spectral correlation at $\alpha = \alpha_k$ which is the cycle frequency being exploited by the TDOA algorithms. The SIR and SNR are both 0 dB and the total SINR is -3 dB. The SPECCORR function $b_\alpha(\tau)$ for $\alpha = \alpha_k$ is shown in Fig. 3(b). It is clear that the dominant peak occurs at the correct TDOA corresponding to the signal of interest. The BL-SPECCORR function is graphed in Fig. 3(c) and it can be seen that the highest peak occurs at the correct TDOA for the signal of interest. The conventional GCC method is particularly inferior when a wide-band interference, which spectrally masks the signal of interest, is present. This is a result of

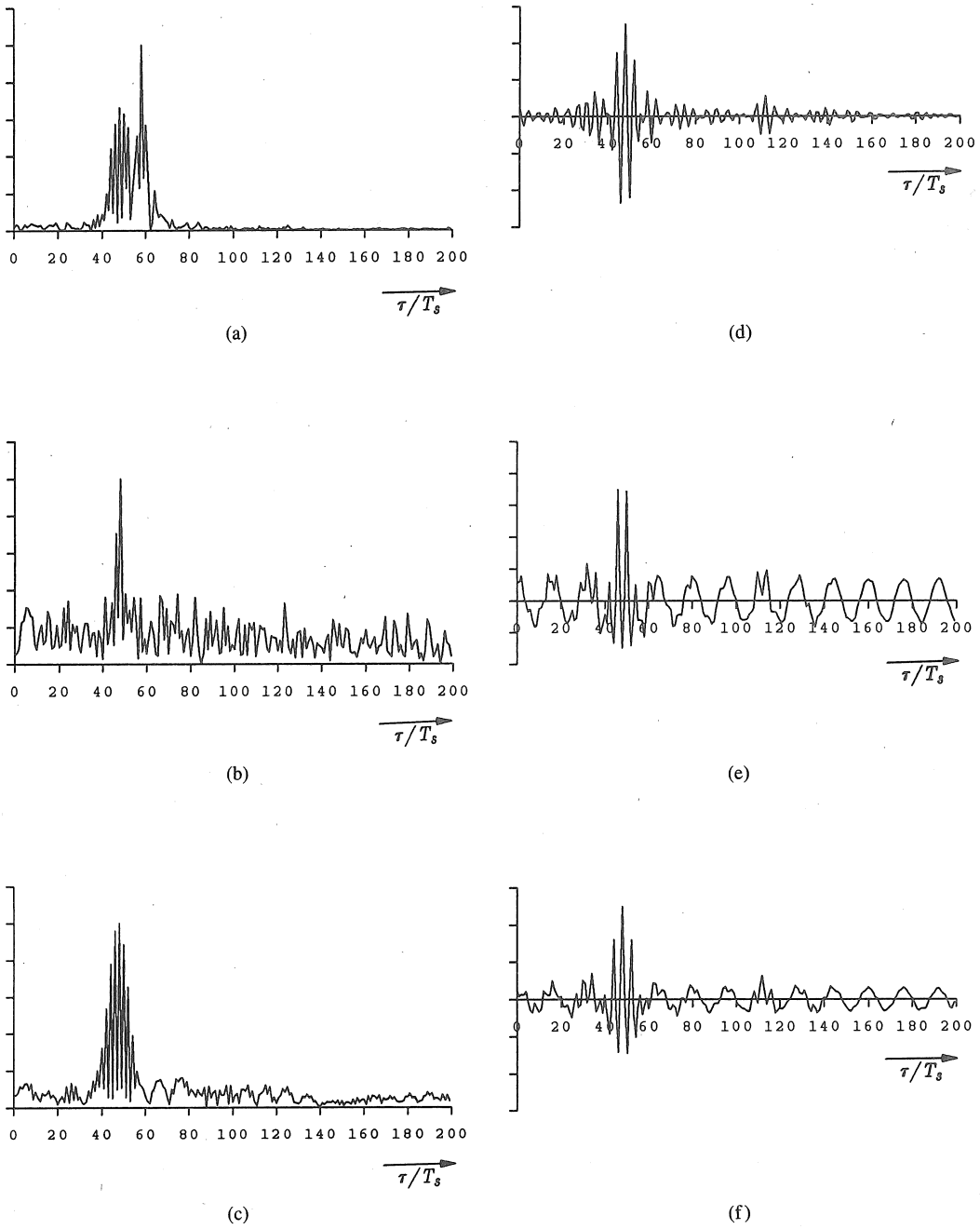

Fig. 3. (a) The GCC function $\hat{b}_0(\tau)$ (without band limiting) for environment 2. The dominant peak occurs at $\tau = \tau_1 = 58T_s$. (b) The SPECCORR function $\hat{b}_\alpha(\tau)$ (without band limiting) for environment 2. The dominant peak occurs at $\tau = D = 48T_s$. (c) The BL-SPECCORR function $\hat{b}_\alpha(\tau)$ for environment 2. The highest peak occurs at $\tau = D = 48T_s$. (d) The SPECCOA function $\hat{c}'_\alpha(\tau)$ for environment 2. The highest peak occurs at $\tau = D = 48T_s$. (e) The SPECCON function $\hat{d}'_\alpha(\tau)$ for environment 2. The lowest null occurs at $\tau = 48T_s$. (f) The PP-SPECCON function $\hat{d}''_\alpha(\tau)$ for environment 2. The highest peak occurs at $\tau = D = 48T_s$.

the fact that i) the phase of $S^0_{yx}(f)$ contains a linear term with slope τ_1, which is the TDOA of the interferer, over a wider band than the term with slope D, and ii) the denominator $S^0_x(f)$, instead of deemphasizing the interference in $S^0_{yx}(f)$, might well deemphasize the signal of interest itself. As a result, $\hat{b}_0(\tau)$ in Fig. 3(a) displays a strong peak at the TDOA $\tau = \tau_1$ of the interferer and a rather weak one at the desired TDOA $\tau = D$. When the bandwidth of the interferer is increased, the performance of the SPECCORR method remains essentially the same, but the performance of the GCC method is degraded.

Because of the increased SINR compared with case 1, the SPECCOA and SPECCON methods perform especially well, as illustrated in Figs. 3(d) and (e), respectively. The PP-SPECCON method is illustrated in Fig. 3(f), where the expected pattern is clearly revealed and the highest peak occurs at the correct TDOA.

C. Environment 3: Coband Interference

The interference in this environment is an AM signal which has a TDOA of $\tau_1 = 58T_s$, and the same carrier

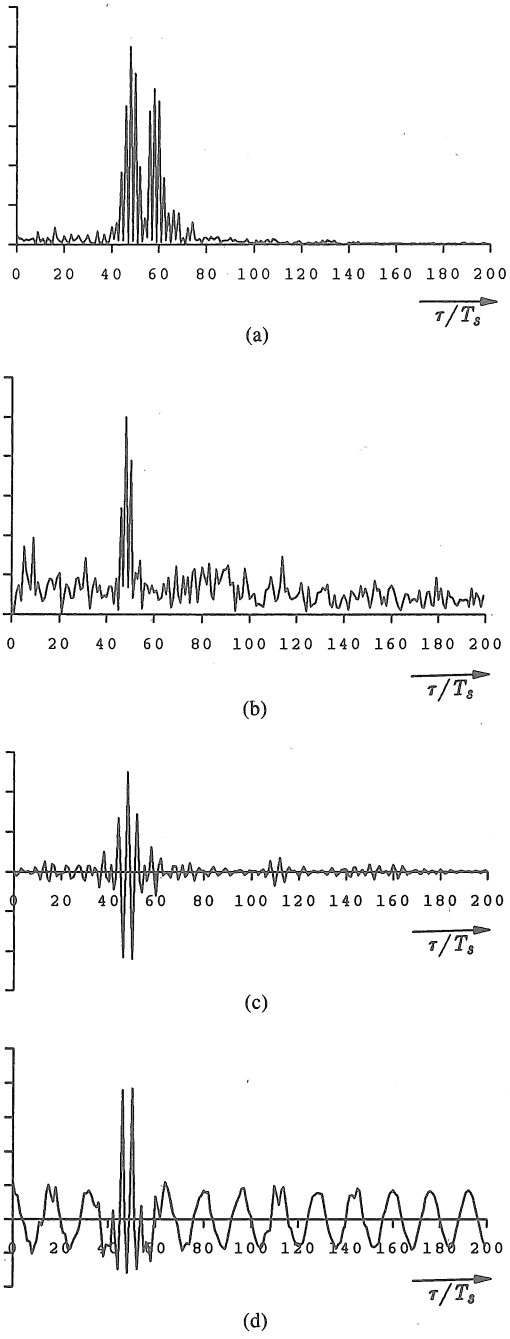

Fig. 4. (a) The GCC function $\hat{b}_0(\tau)$ (without band limiting) for environment 3. The dominant peak occurs at $\tau = D = 48T_s$. (b) The SPECCORR function $\hat{b}_\alpha(\tau)$ (without band limiting) for environment 3. The dominant peak occurs at $\tau = D = 48T_s$. (c) The SPECCOA function $\hat{c}'_\alpha(\tau)$ for environment 3. The highest peak occurs at $\tau = D = 48T_s$. (d) The SPECCON function $\hat{d}'_\alpha(\tau)$ for environment 3. The lowest null occurs at $\tau = 48T_s$.

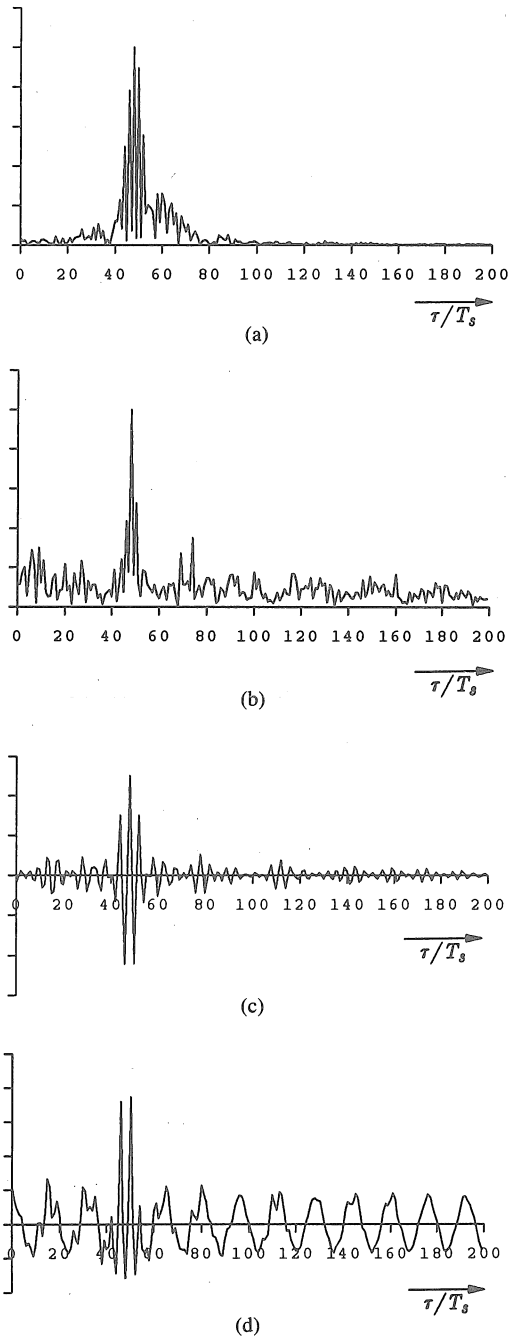

Fig. 5. (a) The GCC function $\hat{b}_0(\tau)$ (without band limiting) for environment 4. The dominant peak occurs at $\tau = D = 48T_s$. (b) The SPECCORR function $\hat{b}_\alpha(\tau)$ (without band limiting) for environment 4. The dominant peak occurs at $\tau = D = 48T_s$. (c) The SPECCOA function $\hat{c}'_\alpha(\tau)$ for environment 4. The highest peak occurs at $\tau = D = 48T_s$. (d) The SPECCON function $\hat{d}'_\alpha(\tau)$ for environment 4. The lowest null occurs at $\tau = 48T_s$.

frequency and bandwidth as that of the BPSK signal of interest. Also, the SIR and SNR are both 0 dB and the combined SINR is -3 dB. The GCC and SPECCORR functions are shown in Figs. 4(a) and (b), respectively. It is clear that the GCC method fails to combat the interference, and either of the two peaks shown in Fig. 4(a) might be taken as the TDOA estimate. On the other hand, the SPECCORR method yields a distinct peak at the correct TDOA.

The SPECCOA and SPECCON functions, shown in Figs. 4(c) and (d), respectively, successfully combat the interference.

D. Environment 4: Narrow-Band Interference

In this last environment, a BPSK signal with carrier frequency of $f_1 = 0.2/T_s$, keying rate of $\alpha_1 = 0.025/T_s$, bandwidth of $B_1 = 0.075/T_s$, and TDOA of $\tau_1 = 58T_s$ is employed as a narrow-band interferer. Again, SIR and SNR are both 0 dB to yield a total SINR of -3 dB. The GCC and SPECCORR functions are shown in Figs. 5(a)

and (b), respectively. Since B_1 is small compared to B_0, the conventional GCC method performs relatively well since it is able to deemphasize the narrow-band interference and to thereby render a strong peak corresponding to the correct TDOA. Nevertheless, since the deemphasis leaves the phase of $S^0_{yx}(f)$ intact, a small peak due to the interferer is still visible. In contrast, no contribution from the interferer is visible for the SPECCORR method. When the bandwidth of the interferer is decreased, the performance of both methods improves (not shown here).

The performance for the SPECCOA and SPECCON methods, illustrated in Figs. 5(c) and (d), respectively, are essentially the same as for the preceding case with the highest peak in the SPECCOA function and lowest null in the SPECCON function positioned at the desired TDOA.

To conclude this qualitative performance assessment, we see that in all four environments, the SPECCORR method consistently outperforms the conventional GCC method, and the TDOA-estimation function $\hat{b}_\alpha(\tau)$ is essentially the same for all cases. This is a result of the relatively large value used for the averaging time T. The SPECCOA and SPECCON methods also consistently outperform the conventional GCC method and require considerably less averaging time than that required by the SPECCOR method. Of course, these results, each of which is based on a single statistical sample, are not necessarily representative of the performance on the average over a number of samples. Nevertheless, these particular results are shown to be representative in the next section, where the results of Monte Carlo simulations are presented.

IV. Quantitative Performance Evaluation

A. Method

To quantitatively assess the performance of the TDOA-estimation methods, we again consider the same simulated BPSK signal of interest in several of the environments described in the previous section, as well as some additional environments, and we compare the MSE's of the TDOA estimates produced by the various methods, as evaluated from Monte Carlo simulations.

We consider first the environments 2 and 4, which consist of wide-band and narrow-band SNOI at 0-dB SIR and WGN at 0-dB SNR. Since the new algorithms perform so well at 0-dB SIR (e.g., yielding normalized MSE's in some cases below -60 dB with a collection of between 1024 and 2048 samples), the case of SIR $= -10$ dB is also considered. Then an interference-free environment with only white Gaussian receiver noise at SNR $= -10$ dB is considered. Since the SPECCOA and PP-SPECCON methods far outperform the conventional GCC method (and all other methods considered) in all these environments, we go on to consider what should be even more challenging situations in the next two cases. In the preceding environments, the closest cycle frequency of the SNOI to that of the SOI differed from that of the SOI by 50%. This motivates the consideration next of a cycle frequency separation of only 1%. It is found that this does somewhat decrease the rate of convergence of MSE (toward its asymptotic value of zero) with increasing collection time, but performance is still excellent (reaching normalized MSEs below -60 dB in some cases with a collection of 2,048 samples). As a final challenge, we consider the situation where the cycle frequency exploited by the algorithm is in error, with respect to the cycle frequency of the SOI, by 1%. Here we find that the GCC method can outperform the new methods when the integration time used exceeds the reciprocal of the cycle frequency error, but even with SNR = SIR = 0 dB, the normalized MSE of the SPECCOA method gets down to -30 dB, before it begins to increase with further increases in integration time.

Since the Cramér–Rao lower bound (CRLB) on the MSE of an unbiased estimator is a standard benchmark against which conventional TDOA estimation methods are often evaluated, it was deemed desirable to also compare the performance of the new methods with this bound. However, the CRLB that is typically used is for a stationary Gaussian SOI in a stationary Gaussian SNOI environment, whereas the environments of primary interest in this paper involve non-Gaussian and nonstationary (cyclostationary) SOI and SNOI. Moreover, the nonstationarity is the primary feature exploited by the new methods. Thus, the conventional CRLB does not apply and, worse yet, the CRLB that does apply is exceedingly difficult to evaluate for non-Gaussian and nonstationary SOI and SNOI. As a compromise, it was decided to compute the conventional CRLB for each environment, treating the SOI and SNOI as if they were Gaussian stationary, and using an SNR in the computation of the CRLB that is equal to the total SINR in the actual environment. The formula used is [4]

$$\text{CRLB} = \frac{3}{8\pi^2 T}\frac{1}{f_2^3 - f_1^3}\left[\frac{2N_0}{S_0} + \left(\frac{N_0}{S_0}\right)^2\right] \tag{27}$$

where S_0 and N_0 are the equivalent flat PSD's of the SOI and SNOI within the band of interest $[f_1, f_2]$, and T is the data collection time. The band of interest was chosen to coincide with the primary band of the SOI:

$$f_1 = f_c - B/2$$
$$f_2 = f_c + B/2 \tag{28}$$

where f_c is the BPSK SOI carrier frequency and B is the null-to-null bandwidth of the BPSK SOI. In all cases considered, the SNR used for this band is either -3 dB (corresponding to either actual SNR = SIR = 0 dB, or actual in-band SNR $= -3$ dB and no interference).

The justification for using this CRLB is that it gives an indication of the best that can be done when cyclostationarity (and non-Gaussianness) of the SOI (and SNOI) is ignored, as is typically done with conventional methods.

In all measured spectral densities used in the various methods, the spectral resolution parameter Δf is equal to

$1/164T_s$, as in Section III. The data collection time T is varied from $T = 256T_s$ to $T = 16\,384T_s$ (which corresponds to a range of from 16 keying intervals of the BPSK SOI to 1024 keying intervals) in increments of 3 dB. Experimentation showed that 400 Monte Carlo trials yielded adequately stable values of MSE up to a point, that is, as long as the normalized MSE remained above about -40 dB. For normalized MSE below -40 dB, a larger number of trials would be necessary, and time interpolation between sample values in the TDOA parameter would be advisable. Although the number of trials was increased to 1000 (the maximum practical value for the computer resources available to this study) for some of the experiments, this value is still too small for reliability below -40 dB.

The MSE's presented are normalized by the squared value of the true TDOA. Thus, -20 dB corresponds to a MSE of 1%, and -40 dB corresponds to 0.01%. The smallest nonzero value of normalized MSE (NMSE) that is measurable with 400 trials for a SOI with TDO$A = 48T_s$ (and no time interpolation) occurs when there is one error equal to one sampling increment T_s in 400 trials, and is given by

$$\mathrm{NMSE}_{\min} = \frac{(T_s)^2}{400}\frac{1}{(48T_s)^2} \cong 10^{-6} \tag{29}$$

which is -60 dB. When the actual NMSE is so small that there are no errors as large as T_s in 400 trials, a value of -80 dB is somewhat arbitrarily assigned, but it is emphasized that values below -40 dB are not reliable. Values below -40 dB are particularly suspect since the correct TDOA value is an integer multiple of the sampling increment. Nevertheless, the value of -80 dB does correctly indicate that MSE is very small indeed, and the results of other simulations (not reported here) where time interpolation was used to accommodate TDOA's not equal to integer multiples of the sampling increment agree well with the results reported here. It is emphasized that normalization of the MSE by the squared TDOA is particularly appropriate since for small MSE's, the root-MSE (RMSE) of the angle of arrival (AOA), using the far-field approximation, is approximately inversely proportional to the maximum TDOA for the platform pair (namely c/L, where c is the speed of propagation and L is the separation between platforms). That is, using the far-field approximation

$$D \cong \frac{L}{c}\sin(\theta) \tag{30}$$

where θ is the AOA, and assuming small RMSE's, we can obtain the approximation

$$\mathrm{RMSE}_\theta \cong \frac{c}{L|\cos(\theta)|}\mathrm{RMSE}_{\mathrm{TDOA}}. \tag{31}$$

B. Results

Fig. 6(a) shows the performance from 400 trials of the SPECCORR method in the wide-band environment 2 and the narrow-band environment 4, each of which has SNR = SIR = 0 dB, and in the modified narrow-band environment 4 with SIR reduced to -10 dB. It can be seen that this method is relatively insensitive to the SNOI, but the sensitivity that is exhibited is greater for an increase in the bandwidth of the SNOI than it is for an increase in the power of the SNOI. That is, the increase in bandwidth by a factor of four results in a larger increase in MSE than does the increase in power by a factor of ten.

Similar behavior is displayed in Fig. 6(b) for 400 trials of the BL-SPECCORR method, except that performance is better overall due to out-of-band noise rejection.

Since the performance of the SPECCOA, SPECCON, and PP-SPECCON methods is so superior to that of the two preceding methods, and since the narrow-band environment is less challenging than the wide-band environment for all methods, Fig. 6(c) shows the performance of these three methods for only the wide-band environment. As an indication of how much better, say, the SPECCOA method is, we note that on the average the SPECCOA method requires only 1/16 the amount of data to perform as well as the SPECCORR method. To confirm this unusual performance, the experiment was modified slightly by changing the carrier frequency of the SNOI from $0.21875/T_s$ to $0.3/T_s$, increasing the number of trials from 400 to 1000, and increasing the maximum collection time from 4096 to 16 384. The results shown in Fig. 6(d) are even better than those in Fig. 6(c). (However, the dip in the MSE of SPECCON has not yet been explained, but it might be a fluke due to insufficient reliability.) In fact, this usually good performance is exhibited even in the WGN-only environment, as shown in Fig. 7. This can be at least partly understood from the fact that these signal-selective methods discriminate against not only interference but also noise (and, more generally, anything that is not cyclostationary with the cycle frequency being used). For the experiment associated with Fig. 7, the SNR in the SOI band is -3 dB and the total SNR (in the entire receiver band) is -10 dB.

As illustrated in Fig. 8, similar performance is achieved by the SPECCOA and PP-SPECCON methods when the cycle frequency of the SNOI is close (within 1% for Fig. 8 instead of the 50% for Fig. 6) to that of the SOI; however, the collection time required to achieve this performance is approximately doubled (cf. Figs. 6(c), (d)). On the other hand, essentially the same performance is achieved by the SPECCORR, BL-SPECCORR, and SPECCON methods, regardless of whether the cycle frequency separation is 1% or 50%. The interference used in obtaining the results in Fig. 8 is similar to that used in the wide-band environment 2: it is a BPSK signal with carrier frequency of $f_1 = 0.23/T_s$, keying rate of $\alpha_1 = \alpha_k + 1/2048T_s \cong 0.06299/T_s$, SNR = SIR = 0 dB, and a TDOA of $\tau_1 = 58T_s$.

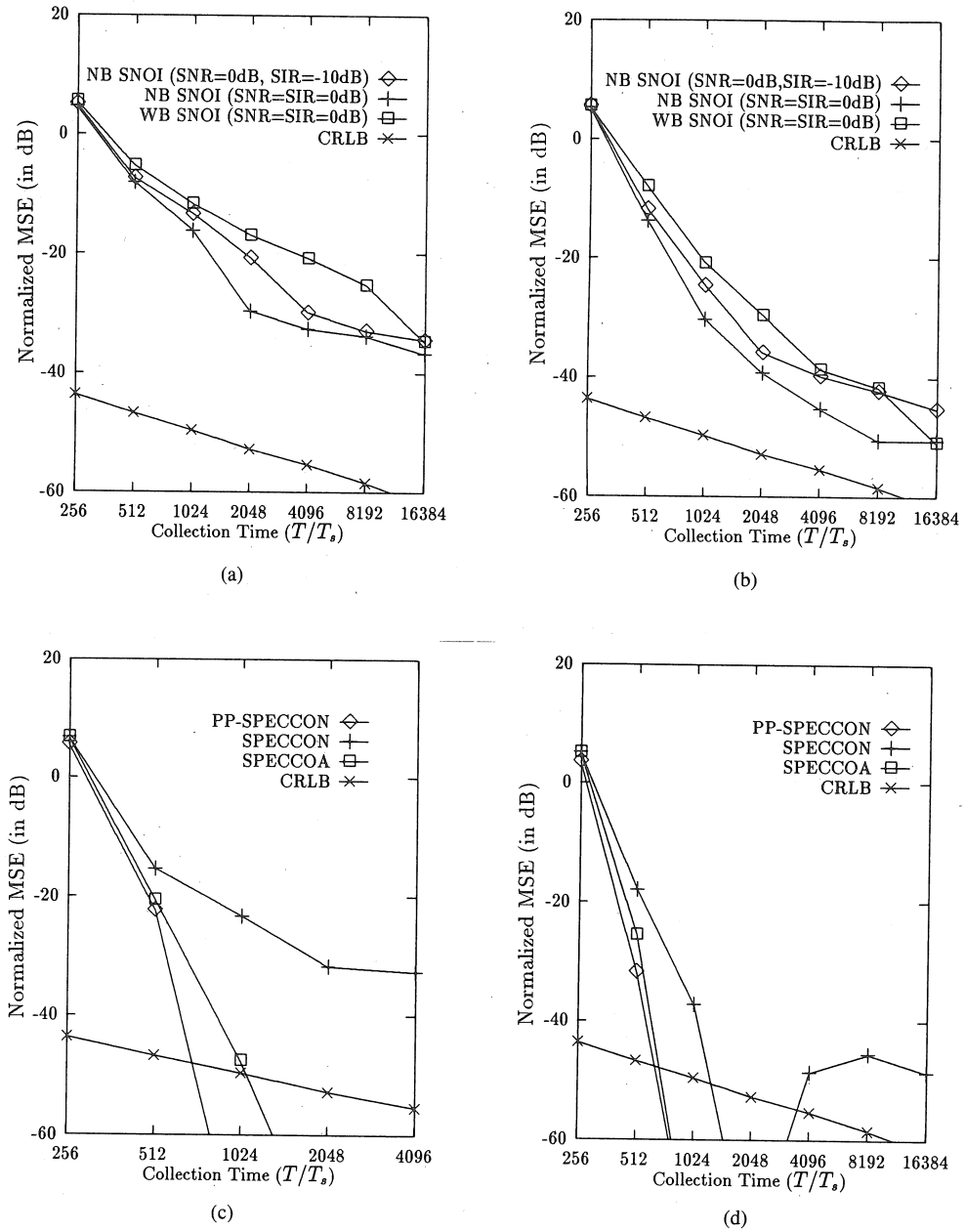

Fig. 6. (a) Normalized MSE versus collection time for the SPECCORR method in three environments. (b) Normalized MSE versus collection time for the BL-SPECCORR method in three environments. (c) Normalized MSE versus collection time for the SPECCOA, SPECCON, and PP-SPECCON methods for the wide-band environment (WB SNOI), environment 2. SNR = SIR = 0 dB. (d) Normalized MSE versus collection time for the SPECCOA, SPECCON, and PP-SPECCON methods for the modified wide-band environment (WB SNOI). SNR = SIR = 0 dB. (In (a)–(d) the CRLB is for a simplified stationary-signal model.)

In the last experiment to be considered, the coband environment 3 from Section III, where SNR = SIR = 0 dB, is adopted, but the cycle frequency used by the algorithms is in error by 1%: $|\alpha - \alpha_k| = 0.00625/T_s$. As shown in Fig. 9, for collection times up to between 1024 and 2048, the performances of the SPECCORR, BL-SPECCORR, and SPECCOA methods are very similar to their performances in previous cases where there is no cycle frequency error. However, when the collection time T exceeds this range, it exceeds the reciprocal ($1600T_s$) of the cycle-frequency error, that is, the cycle-frequency resolution width $\Delta\alpha \cong 1/T$ becomes smaller than the cycle frequency error. As a result, performance continually degrades as collection time is increased beyond this point. As shown in Fig. 10, for each method the mean of the TDOA estimate decreases rapidly to the vicinity of the true TDOA value (within less than 1% in the best case) and the standard deviation drops drastically (to less than 4% in the best case) as collection time increases from $256T_s$ to $512T_s$. Then, with further increases in collection time from $512T_s$ to $16\,384T_s$, the mean error (bias) increases only slowly (about three orders of magnitude more slowly than the MSE decreases). Thus, the methods do not fail catastrophically: the bias is only about 10% and

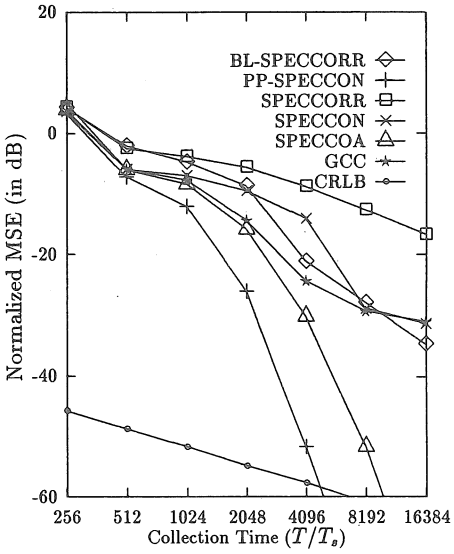

Fig. 7. Normalized MSE versus collection time for the SPECCORR, BL-SPECCORR, SPECCOA, SPECCON, PP-SPECCON, and GCC methods in a WGN environment with SNR = −10 dB. (The CRLB is for a simplified stationary-signal model.)

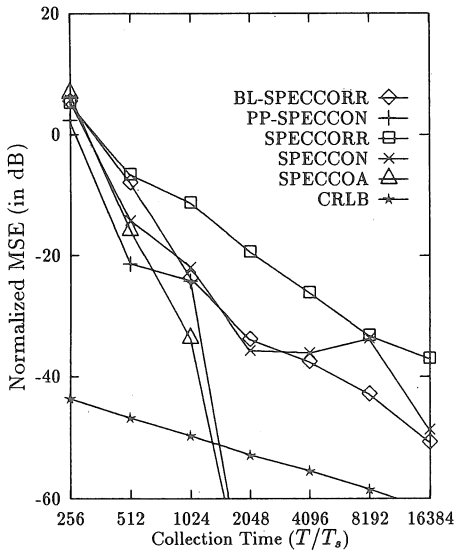

Fig. 8. Normalized MSE versus collection time for the SPECCORR, BL-SPECCORR, and SPECCOA methods, when the cycle frequency of the SNOI is within 1% of that of the SOI (WB SNOI). SNR = SIR = 0 dB. (The CRLB is for a simplified stationary-signal model.)

the standard deviation is about 10% to 20% even when collection time, 16 384T_s, is ten times the critical value of 1600T_s, which is the reciprocal of the cycle frequency error.

V. Conclusion

In conclusion, the new signal-selective algorithms exhibit excellent robustness for BPSK signals in a wide range of interference and noise environments and operating conditions. Results not reported here show the same level of performance for QPSK signals, and experimentation with other signal types such as FSK suggests that comparable

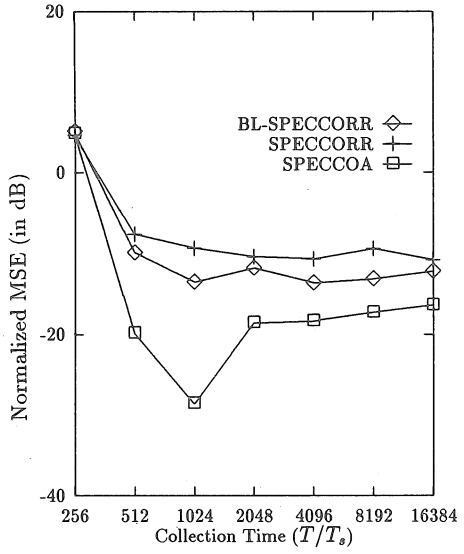

Fig. 9. Normalized MSE versus collection time for the SPECCORR, BL-SPECCORR, and SPECCOA methods for the coband environment when cycle frequency is in error by 1%. (Coband SNOI.) SNR = SIR = 0 dB.

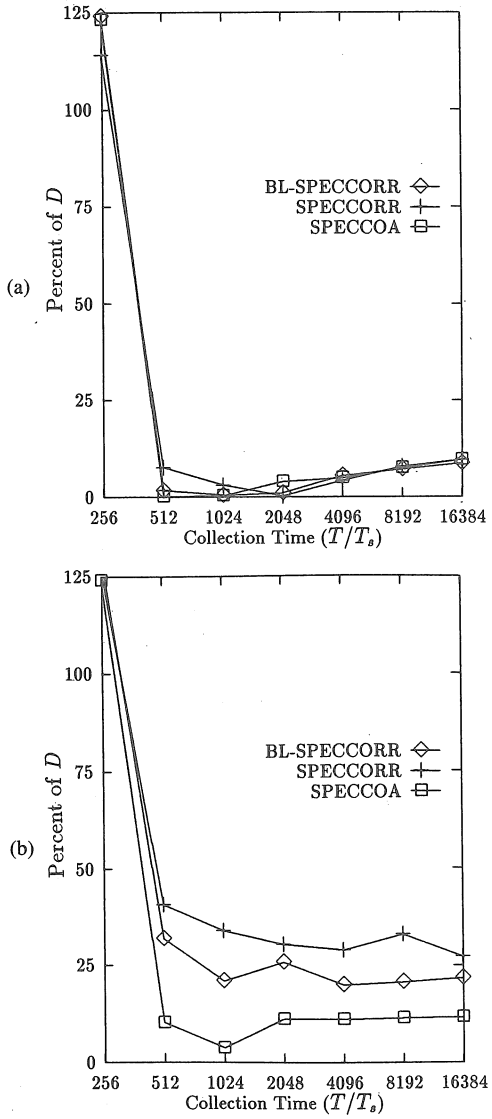

Fig. 10. (a) Normalized bias β in percent of correct TODA D, versus collection time for 1% error in cycle frequency α. (b) Normalized standard deviation σ in percent of correct TDOA D, versus collection time for 1% error in cycle frequency α.

performance is attainable in those cases where the signals of interest exhibit substantial spectral correlation. These new algorithms are tolerant to both interfering signals and noise, and they can outperform conventional algorithms that achieve the Cramér–Rao lower bound on variance for stationary signals because the signals considered here are nonstationary (cyclostationary) and the algorithms exploit the nonstationarity to discriminate against noise and interference. The most important issue regarding signal type and corresponding performance that has been discovered so far is the strength of the signal's cyclic feature (or spectral correlation feature) to be exploited, which is related to the degree of cyclostationarity in the signal (cf. [5]). For example, bandwidth-efficient digital signals can have relatively weak keying-rate features in the sense that the proportionality factor—the spectral coherence function $C_s^\alpha(f)$—in (18) is close to unity over only a relatively small band. This limits the band over which the linear phase-versus-frequency characteristic of the spectral correlation functions can be used, thereby limiting reliability of the estimate of the slope of this line. Although this can in principle always be compensated for by increasing the collection time (cf. (18)), there are of course practical limits to this.

Acknowledgment

The authors gratefully acknowledge the assistance of Dr. S. V. Schell and C. M. Spooner in establishing repeatability of the simulation results and refining the graphical display of results.

References

[1] W. A. Gardner and C. K. Chen, "Signal-selective time-difference-of-arrival estimation for passive location of man-made signal sources in highly corruptive environments, Part I: Theory and method," *IEEE Trans. Signal Processing*, this issue, pp. 1168–1184.

[2] W. A. Gardner, *Statistical Spectral Analysis: A Nonprobabilistic Theory*. Englewood Cliffs, NJ: Prentice-Hall, 1987.

[3] W. A. Gardner, "Measurement of spectral correlation," *IEEE Trans. Acoust., Speech, Signal Processing*, vol. ASSP-34, no. 5, pp. 1111–1123, Oct. 1986.

[4] C. H. Knapp and G. C. Carter, "The generalized correlation method for estimation of time delay," *IEEE Trans. Acoust., Speech, Signal Processing*, vol. ASSP-24, pp. 320–327, Aug. 1976.

[5] G. D. Zivanovic and W. A. Gardner, "Degrees of cyclostationarity and their application to signal detection and estimation," *Signal Processing*, vol. 22, pp. 287–297, 1991.

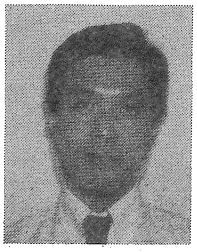

Chih-Kang Chen (S'82–M'89) received the B.S. degree from California State University, Sacramento, in 1983 and the M.S. and Ph.D. degrees from the University of California, Davis, in 1985 and 1989, respectively, all in electrical engineering.

From April 1989 to February 1990, he was a postdoctoral fellow at the University of California, Davis, performing research work in the area of signal detection and parameter estimation. Since February 1990 he has been with Silicon Engines developing fully digital real-time spectrum analyzers for NASA's Search for Extra-Terrestrial Intelligence (SETI) project. His research interests include signal detection and estimation and digital signal processing. He is the coauthor (with W. A. Gardner) of *The Random Processes Tutor: A Comprehensive Solutions Manual for Independent Study* (McGraw-Hill, 1990).

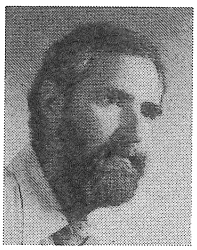

William A. Gardner (S'64–M'67–SM'84–F'91) was born in Palo Alto, CA, on November 4, 1942. He received the M.S. degree from Stanford University in 1967 and the Ph.D. degree from the University of Massachusetts, Amherst, in 1972, both in electrical engineering.

He was a Member of the Technical Staff at Bell Laboratories in Massachusetts from 1967 to 1969. He has been a faculty member at the University of California, Davis, since 1972, where he is Professor of Electrical Engineering and Computer Science. Since 1982, he has also been President of the engineering consulting firm Statistical Signal Processing, Inc., Yountville, CA. His research interests are in the general area of statistical signal processing, with primary emphasis on the theories of time-series analysis, stochastic processes, and signal detection and estimation. He is the author of *Introduction to Random Processes with Application to Signals and Systems* (Macmillan, 1985; second edition, McGraw-Hill, 1990), *The Random Processes Tutor: A Comprehensive Solutions Manual for Independent Study* (McGraw-Hill, 1990), and *Statistical Spectral Analysis: A Nonprobabilistic Theory* (Prentice-Hill, 1987). He holds several patents and is the author of numerous research-journal papers.

Dr. Gardner received the Best Paper of the Year Award from the European Association for Signal Processing in 1986 for the paper entitled "The Spectral Correlation Theory of Cyclostationary Signals," the 1987 Distinguished Engineering Alumnus Award from the University of Massachusetts, and the Stephen O. Rice Prize Paper Award in the Field of Communication Theory from the IEEE Communications Society in 1988 for the paper entitled "Signal Interception: A Unifying Theoretical Framework for Feature Detection." He is a member of the American Mathematical Society, the American Association for the Advancement of Science, and the European Association for Signal Processing, and a member of the honor societies Sigma Xi, Tau Beta Pi, Eta Kappa Nu, and Alpha Gamma Sigma.